AGU ADVANCING EARTH AND SPACE SCIENCE

Geophysical Research Letters

RESEARCH LETTER
10.1029/2022GL102395

Adapting to a Foggy Future Along Trans-Arctic Shipping Routes

Shutong Song[1,2], Yue Chen[1,2,3], Xianyao Chen[1,2], Changshuo Chen[4], King-Fai Li[5], Ka-Kit Tung[6], Qiuli Shao[2], Yilin Liu[1], Xiaoyu Wang[1], Li Yi[1], and Jinping Zhao[1,2]

[1]Frontier Science Center for Deep Ocean Multispheres and Earth System (FDOMES), Physical Oceanography Laboratory, Ocean University of China, Qingdao, China, [2]Qingdao National Laboratory for Marine Science and Technology, Qingdao, China, [3]Academy of the Future Ocean, Ocean University of China, Qingdao, China, [4]Geovis Technology Company Limited, Beijing, China, [5]Department of Environmental Sciences, University of California, Riverside, Riverside, CA, USA, [6]Department of Applied Mathematics, University of Washington, Seattle, WA, USA

Abstract Rapid retreat of Arctic sea ice extends the area of open ocean for new trans-Arctic shipping routes. However, the projected routes may be too optimistic in terms of savings in shipping costs from shortened trans-Arctic distances as they do not consider the increased sea fog frequency (SFF) over areas of the retreating sea ice. We show that delays due to sea fog can be 1–4 days, about 23%–27% along the Northwest Passage and 4%–11% along the Northern Sea Route than previous estimated. We design a route based on the projected sea-ice extent and SFF. The new route can reduce the sailing time by 0.3–1 day by detouring the routes with lighter impacts of sea fog. More importantly the new route will lower the risk of catastrophic accidents compared to the shortest route and saves the additional costs due to unscheduled port calls.

Plain Language Summary Rapid loss of sea ice under global warming opens up the Arctic Ocean to shipping. The available trans-Arctic shipping in the near future will strongly decrease sailing time and financial costs from the Far East to Northwest Europe. Previous designs of trans-Arctic shipping routes mainly considered sea ice distribution, but ignored the important effect of frequent and high-risk polar sea fog. Here, we project Arctic sea fog frequency in 21st century and evaluate its influence on trans-Arctic shipping routes. The results highlight the necessity to redesign the routes by including sea fog effect for safer ship navigation.

Key Points:

- About 20%–30% of Arctic shipping routes experience frequent sea fog frequency more than 20%
- Sea fog increases the shipping time by 23%–27% along the Northwest Passage and 4%–11% along the Northern Sea Route than previous estimations
- Shipping routes by minimizing the impacts of sea fog can save 0.3–1 days sailing time by detouring dense-sea-fog region

Supporting Information:

Supporting Information may be found in the online version of this article.

Correspondence to:

X. Chen,
chenxy@ouc.edu.cn

Citation:

Song, S., Chen, Y., Chen, X., Chen, C., Li, K.-F., Tung, K.-K., et al. (2023). Adapting to a foggy future along trans-Arctic shipping routes. *Geophysical Research Letters*, *50*, e2022GL102395. https://doi.org/10.1029/2022GL102395

Received 6 DEC 2022
Accepted 13 MAR 2023

1. Introduction

The increase of open water area as a result of sea-ice retreat has boosted socio-economic developments in the Arctic, such as oil extraction, Arctic tourism, and trans-Arctic shipping routes (Gössling & Hall, 2006; Stroeve et al., 2008; Theocharis et al., 2018). The latter has particularly received more international interest after the 2021 Suez Canal Blockage. Ship companies can realize the greatest advantage because present travels of more than 20,000 km from the Far East to Northwest Europe via the Suez Canal can be reduced to about 10,000 km and the average sailing times can be shortened from 20 days in the 1990s to 11 days on average in 2012–2013 if either the Northern Sea Route (NSR) via north of the Russian Federation through the Arctic or the Northwest Passage (NWP) via the Canadian Arctic Archipelago are used (Nordquist et al., 2010; Schøyen & Bråthen, 2011). Taking into account canal fees, fuel costs, and other variables that determine freight rates, this shortcut can tremendously reduce the costs of a large container ship company every year. The cost savings would be even higher for ships that are too large to pass through Panama and Suez Canals and so currently still sail around the Cape of Good Hope and Cape Horn (Hong, 2012). However, the occurrence of fog may slow down or even stop these marine operations in the ocean with floating ice, leading to significant economic costs (Buixadé Farré et al., 2014). Vessels equipped with cutting-edge instruments such as radar, searchlights, and radios can reduce but not avoid collisions. Even the highly instrumented ice-breaker *R.V. Xuelong* collided with an iceberg in thick fog during its 35th voyage. In the open ocean without sea ice, sea fog has little impact on the speed of the ship. However, when encountering sea fog in sea-ice area, common open-water (OW) and even Polar Class 6 (PC6) vessels have to reduce their speeds by nearly 40% to increase navigational safety (Figure S1 in Supporting Information S1). Previous assessments of future optimal navigation routes in the Arctic are primarily based on sea ice conditions under the representative concentration pathway (RCP) 4.5 and 8.5 climate-forcing scenarios (Li et al., 2020; Melia et al., 2016; Smith & Stephenson, 2013; Wei et al., 2020). It is worth noting that the impact of sea ice drift and growler icebergs is included in the changing sea ice conditions composed by sea ice thickness and sea ice

concentration (Marko et al., 1982; Wagner et al., 2021). In order to assess the impact of sea fog on the potential shipping routes, we use a combination of present-day reanalysis and model simulations to project sea fog variability in 21st century and design new routes based on sea ice and sea fog changes.

2. Data and Methods

2.1. Data

Observations from International Comprehensive Ocean-Atmosphere Data Set (Freeman et al., 2017) are used to obtain Arctic sea fog during 1979–2018.

The 6-hourly daily ERA-Interim from European Centre for Medium-Range Weather Forecasts (Dee et al., 2011) during 1979–2018 are used as initial and boundary conditions to estimate the occurrence of fog in a regional climate model.

Sea ice concentration and sea ice thickness of Ocean Reanalysis System 5 (ORAS5) are used to represent historical sea ice conditions, as the atmospheric forcing is from ERA-Interim.

To project the future sea ice and sea fog, we use monthly sea ice concentration, sea ice thickness, relative humidity (RH) and atmospheric stability (defined as the temperature inversion between 925 hPa and 2 m above ground) from climate models in the Fifth Phase of the Coupled Model Intercomparison Project (CMIP5) during 1979–2005 from historical experiment and during 2006–2099 under RCP4.5 and 8.5. In order to reduce the inter-model bias on sea fog simulation, we choose six "best" models in CMIP5, which can well capture the historical sea fog frequency (SFF) in the Arctic (see Text S1 in Supporting Information S1). They are ACCESS1-0, HadGEM2-CC, CanESM2, GISS-E2-R, GISS-E2-R-CC, and GISS-E2-H.

2.2. Model Simulated Fog Results and the Definition of Fog

We use the Polar-optimized version of the Weather Research and Forecasting Model (PWRF) (Bromwich et al., 2009) to simulate the liquid water content in bottom model level and then apply the fog-diagnostic scheme suggested by Stoelinga and Warner (1999) to determine whether fog occurs (see Text S2 in Supporting Information S1). Direct simulation of sea fog in this way requires 6-hourly atmospheric fields, with at least 25-hPa vertical resolution within the boundary layer, as the initial and boundary conditions. This kind of data is usually unavailable in future projections based on the CMIP5. To project the future Arctic sea fog variability, we first simulate the historical Arctic SFF during 1979–2018 using PWRF with 6-hourly atmospheric fields from ERA-Interim reanalysis data sets (PWRF-ERA). Then we derive a semi-empirical multi-variable linear relationship between the Arctic SFF with the RH and atmospheric stability based on this hindcast simulation (see Text S3 in Supporting Information S1). We note that though the Arctic will experience a new climate state in the future (Landrum & Holland, 2020), the historical relationship between SFF, RH, and atmospheric stability remains reasonable well in the future scenario (Figure S2 in Supporting Information S1). Finally, the future Arctic SFF is estimated using the CMIP5 multi-model ensemble means RH and atmospheric stability and the derived semi-empirical relationships.

We define SFF as the fraction of Arctic sea fog days in each summer (July–September) (Hanesiak & Wang, 2005; Sugimoto et al., 2013). A day is defined as fog day, if at least one 6-hourly model output in this day is foggy. Based on the simulations of PWRF-ERA, the SFF is highly correlated ($\geq$0.7) with the RH over most of the Arctic Ocean except the north Beaufort Sea (Figure S3 in Supporting Information S1). The strong correlation between SFF and RH is expected because high RH, which means that the atmosphere approaches 100% more frequently (Figure S4 in Supporting Information S1), is a necessary (but not sufficient) condition for the onset of fog (Isaac et al., 2020). Atmospheric stability is another necessary condition for the onset of fog over the north Beaufort Sea, where the atmospheric stability is shown to be well correlated with SFF (~0.4; Figure S3 in Supporting Information S1). The simulation suggests that a northward-propagating Beaufort high-pressure center enhances local atmospheric stability while an eastward-propagating Beaufort high enhances the local RH (Figure S5 in Supporting Information S1).

3. Arctic Sea Fog Change

The climatological SFF derived from the PWRF-ERA shows that the SFF along the coast is higher than 20%, and less than 6% in the central Arctic (Figures 1a and 1b). This spatial distribution is similar to observations and previous studies (Eastman & Warren, 2010; Koračin & Dorman, 2017). The historical SFF over the Arctic Ocean

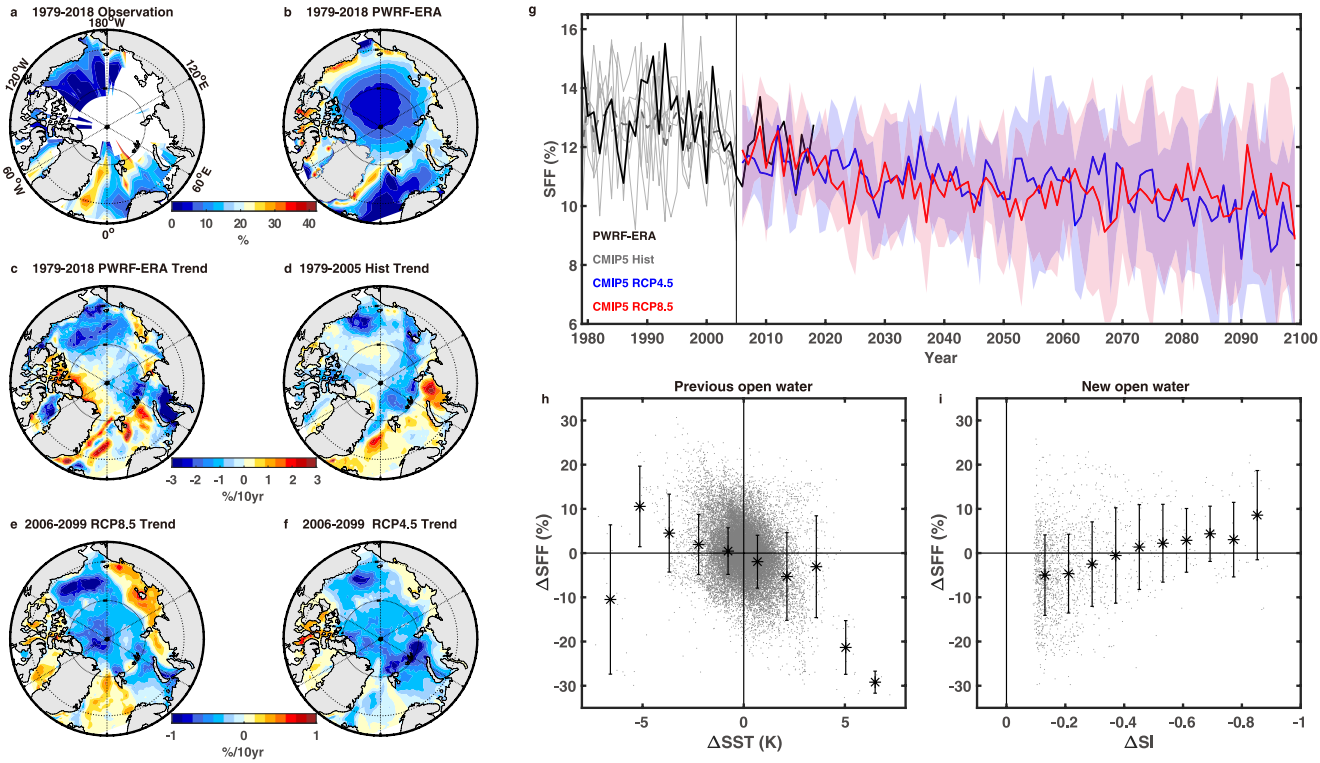

Figure 1. Climatological distribution of summertime Arctic sea fog frequency (SFF). (a) and (b) are the SFF climatology derived from ship observations and the PWRF-ERA, respectively. The shaded grid in (a) represents observation with data more than 10 years. (c), (d) are spatial pattern of the linear trend of the SFF derived from the PWRF-ERA and the historical run of the Coupled Model Intercomparison Project (CMIP5) models during 1979–2018. (e) and (f) are the linear trend of the projected SFF under RCP4.5 and 8.5 scenarios during 2006–2099. (g) Shows the time series of regional averaged SFF over the ocean north of 70°N based on PWRF-ERA (black), the historical CMIP5 (gray), the RCP4.5 (blue) and 8.5 (red). Shading indicates ± one standard deviation. (h) Shows the fog change and SST change over regions which are open water in previous and current years. Error bars show the mean and one standard deviation. (i) Is the relationship between fog and sea ice change over regions where sea ice in the previous year is larger than 10% but melts into open water in the current year (sea ice less than 1%). (h) and (i) are based on PWRF-ERA.

north of 70°N during the past 40 years simulated by the PWRF-ERA exhibits a decreasing trend in the central Arctic and increasing trend along the coast (Figure 1c). The regional mean SFF during 1979–2005 is decreasing with the rate of −0.44% ± 0.21% every decade (Figure 1g), because the saturation vapor pressure increases faster than the partial pressure of water vapor, especially over the open water area (Figure 1h). However, the SFF increases significantly over the newly open water regions (Figure 1i) due to the increasing moisture and latent heat exchange between the air and the relatively warm sea surface (Bintanja & Selten, 2014). Notably, the SFF usually increases substantially over the new open water regions where sea ice concentration is more than 40% in the previous year (Figure 1i). These new open water regions are often chosen as the new shipping routes (Smith & Stephenson, 2013) because of the shorter distances, but the impact of increased fog events have not been considered in those studies.

The well-chosen CMIP5 models (see Text S1 in Supporting Information S1) can capture the spatial structure of the linear trend of the historical SFF variability (Figures 1d and 1g). The decreasing trend of the ensemble-mean SFF is −0.35% ± 0.18% during 1979–2005. In future, the decreasing trend of the SFF is −0.18% ± 0.03% during 2006–2099 under both RCPs. But spatially, the SFF increases along the coastal area (Figures 1e and 1f), which will exert significant impacts on the ship activities in this area.

4. Impacts of Sea Fog on the Shipping Routes

4.1. Historical Period

We may estimate the impacts of sea fog on the transit time along the shipping routes using the hindcast simulations during 2000–2018. Previous studies have designed trans-Arctic routes based on the capability of PC6 and

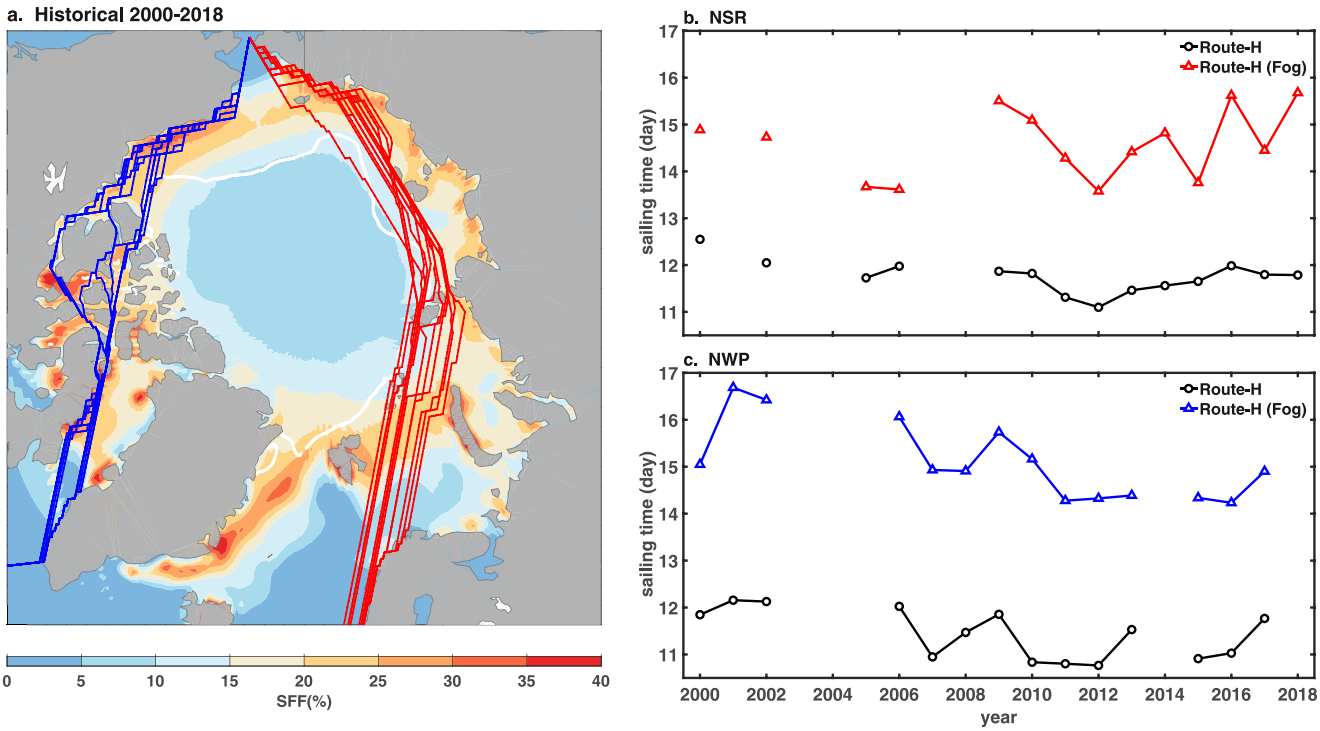

Figure 2. Navigation routes for hypothetical ships to cross the Arctic Ocean along Northern Sea Route (NSR) and North West Passage (NWP) during 2000–2018. (a) Red and blue line represents the Route-H of NSR and NWP every year, respectively. White line indicates the isopleth of 45% sea ice concentration. Simulated sea fog frequency are shaded. (b) and (c) are total sailing time along NSR and NWP respectively. The line with circle markers indicates the Route-H only based on sea ice conditions; The line with triangle markers indicates the Route-H considering the deceleration of sea fog. The gap means that no route is available due to sea ice cover.

OW vessels for medium-to-low sea ice conditions (Li et al., 2020; Melia et al., 2016; Smith & Stephenson, 2013; Wei et al., 2020). We employ the same method to derive the trans-Arctic routes from July to September for a container ship with moderately ice-strengthened PC6 (Table S2 in Supporting Information S1), which is used in more than half of the global seaborne trade with diverse types of commodities transported (Ducruet, 2013; Munim et al., 2022).

Figure 2a shows the derived shipping routes for hypothetical ships crossing the Arctic Ocean, starting from Rotterdam or St. John's and terminating at Bering Strait (hereafter referred as Route-H). If only the impact of sea ice is considered, the sailing time along Route-H is about 12 days (Figures 2b and 2c). The total distance of Route-H is about 8,150 km for NSR and 7,960 km for NWP.

To show the SFF along the Route-H, we use the cumulative distance traveled from Rotterdam or St. John's as the abscissa along the route (Figure S6 in Supporting Information S1). NSR experienced frequent sea fog during 2000–2018. There is more than 1,850 km of the voyage along NSR with SFF exceeding 20% (defined as a high-SFF region). The maximum SFF can reach 36%. Compared with NSR, sea fog along the NWP is more frequent, more than 2,690 km of high-SFF region. The maximum SFF can reach 45%.

To quantify the impacts of sea fog on Route-H, we introduce a deceleration coefficient to account for the fact that ships need to slow down sailing in sea fog (Text S4 and Table S4 in Supporting Information S1). The higher SFF along the route, the larger deceleration coefficient will be. We estimate that the total sailing time along the NSR and the NWP will increase by about 1.6–3.9 and 2.9–4.5 days when the impacts of sea fog are considered (Figure 2), which is 10%–40% of the average sailing time.

4.2. Future

We investigate the impacts of sea fog on the potential trans-Arctic routes in the future under the projections with the significant melt of Arctic sea ice. We derive the routes from July to September in nine non-overlapping 10-year segments from 2006 to 2095, using CMIP5 multi-model ensemble means of sea ice under RCP4.5 and

8.5 (hereafter referred as Route-I). Route-I is also planned for a container ship with moderately ice-strengthened PC6 (Table S2 in Supporting Information S1).

Consistent with the previous plans, the Route-I tends to shift to higher latitudes and will go through the central Arctic Ocean by midcentury under the Arctic warming (Figure 3). Due to the shorter sailing distance, the sailing time of Route-I decreases from 11 days during 2006–2015 to 10 days during 2086–2095 along the NSR, and decreases from 12 to 11 days along the NWP (Figure 4).

The high SFF region along the NSR (Figure 5a) is in the Fram Strait (2,900–3,400 km) and the Chukchi Sea (6,400–7,000 km). The maximum SFF along the NSR reaches more than 25% during 2006–2015, as the route approaches the Eurasian coast. The high-SFF region reduces from 530 km during 2006–2015 to 185 km during 2086–2095. Along the NWP, the maximum SFF is about 35%, located in the Baffin Bay (3,000–3,700 km) and the Beaufort Sea (6,000–7,000 km). The high-SFF region can reach about 2,350 km during the 21st century (Figure 5b). These results are similar between RCP4.5 and 8.5.

Both the NSR and the NWP are inevitably affected by sea fog in the 21st century. Sea fog along the NWP is more frequent and persistent, which will increase the sailing time by 2.5–3 days, about 23%–26% than previous estimations (Figure 4). Along the NSR, the impact of sea fog is relatively weaker but the sailing time will still increase 0.5 day due to the high-SFF in some regions. Therefore, designing an optimal route to avoid heavy fog regions should be part of the voyage plan.

5. Re-Designing Shipping Routes by Minimizing the Impacts of Sea Fog

Can we reduce the delays by detouring from some sea fog regions? We re-optimize the Route-I using a cost function that considers the change of the cruising speeds under different sea-fog and sea-ice conditions. The cost function is minimized with respect to the sailing time. Thus, the new route, referred to as Route-F, has the shortest sailing time (GEF-UNDP-IMO GloMEEP Project and members of the GIA, 2020) (Text S4 and Figure S7 in Supporting Information S1). Based on the CMIP5 multi-model ensemble means of sea ice and the SFF, we compute the path and the sailing time of the Route-F every 10 years in 21st century under both RCPs.

Along the NWP, the Route-F can gain back 0.3–1 days of sailing time compared to the Route-I (Figure 4b), albeit it is longer. The Route-F through the Canadian Arctic Archipelago is similar to the Route-I because of the island locations; the major detours are the northward shifts of the Route-F relative to the Route-I along the Alaska coastline to avoid high-SFF regions (Figure 3). The shift along the Alaska coast segment (6,000–7,000 km) becomes gradually obvious due to the retreat of sea ice over the Beaufort Sea before the midcentury. After the midcentury, the impacts of the SFF becomes dominant. By the end of this century, the SFF over this segment will decrease by 10%–13% (Figure 5d). Although the length of the Route-F is longer than the Route-I, the decrease in sea fog along the Route-F helps for saving the sailing time up to 1 day. In RCP4.5, with the high-SFF region along the NWP, the routes between St. John's and Bering Strait switch the transit via the NSR during 2026–2035 and 2056–2065 (Figure S8 in Supporting Information S1). Although the routes are about 1,000 km longer than the NWP through the Canadian Arctic Archipelago, the high-SFF region is reduced by 1,260 km (Figure S9 in Supporting Information S1).

In contrast, along the NSR, the Route-F can only gain back 0.1–0.4 days of sailing time compared to the Route-I (Figure 4). The Route-F tends to avoid high-SFF region along the Eurasian coast to navigate at higher latitudes during the first half of the century. After the midcentury, the Route-F tends to avoid the northeast coast of Greenland and shifts eastward to the Fram Strait. The route no longer passes through the high-SFF region by the end of this century. The detour of Route-F is similar under RCP4.5 (Figures S8 and S9 in Supporting Information S1).

We further compare the Route-F with the traditional routes such as the Suez Canal and the Panama Canal (Table S5 in Supporting Information S1). These routes start from Shanghai and terminate at St. John's and Rotterdam. The result shows that the Route-F of NSR or NWP can still save 30%–33% of the distance and 20%–30% of the time of traditional routes on average in the 21st century, suggesting great economic benefits of the Route-F.

6. Conclusions

Previously designed shipping routes based on the shortest distance are not necessarily the safest routes because the presence of sea fog along the routes has not been considered. For safety, the captain may reduce the cruising

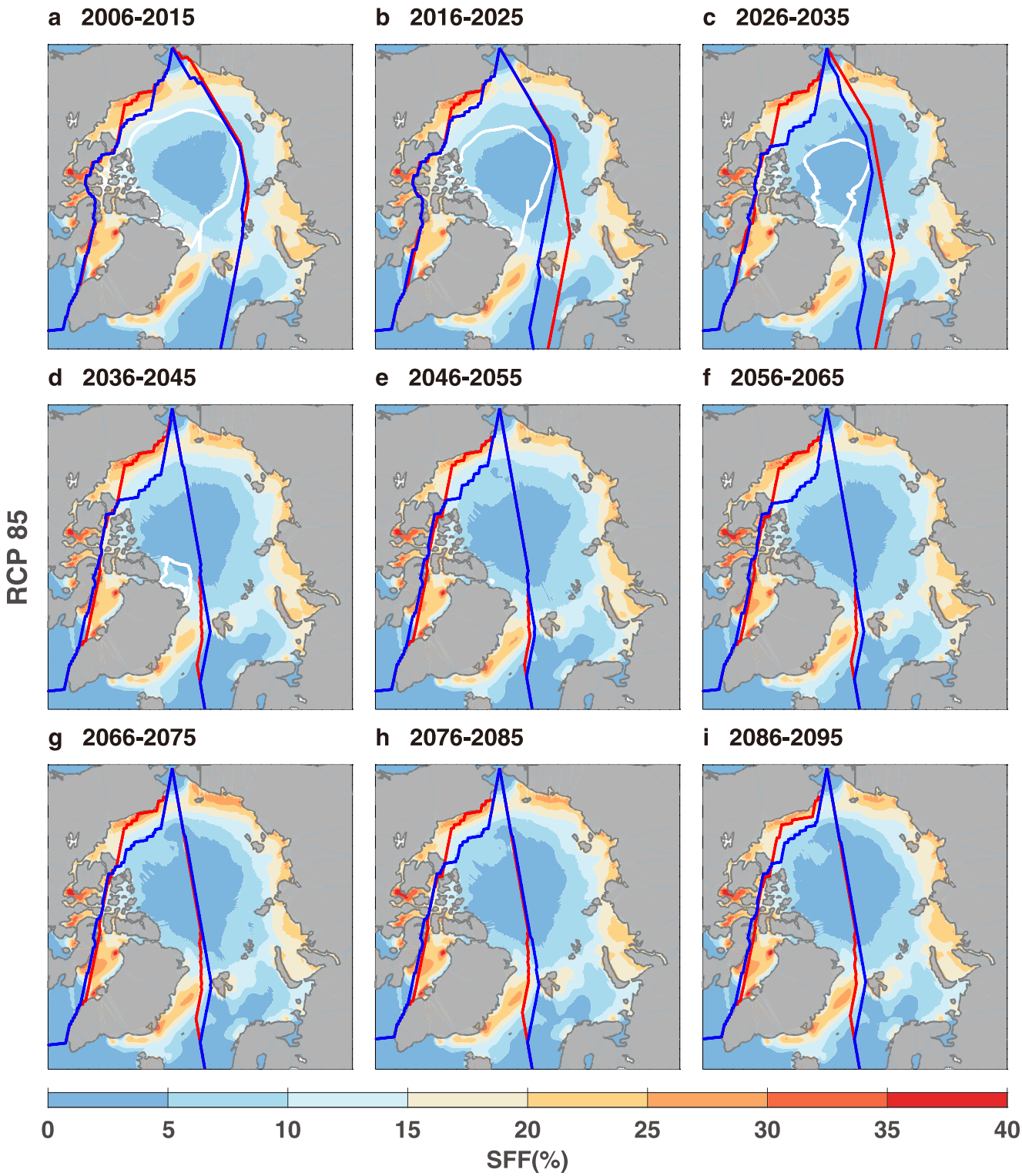

Figure 3. The routes along Northern Sea Route and Northwest Passage every decade under RCP8.5. Red and blue lines represent Route-I and Route-F, respectively. White line is the isopleth of 45% sea ice concentration. Projected sea fog frequency are shaded.

speed when sailing in sea fog. By parameterizing the captain's decision as a reduction of the cruising speed in sea fog, we found that the sailing time of the shortest routes should have been 5%–25%, or 1–4 days, more than previously estimated. Our finding is particularly important along newly formed sea-ice margins, not only because a safe voyage is more difficult along the margins, but also because sea fog here is projected to be

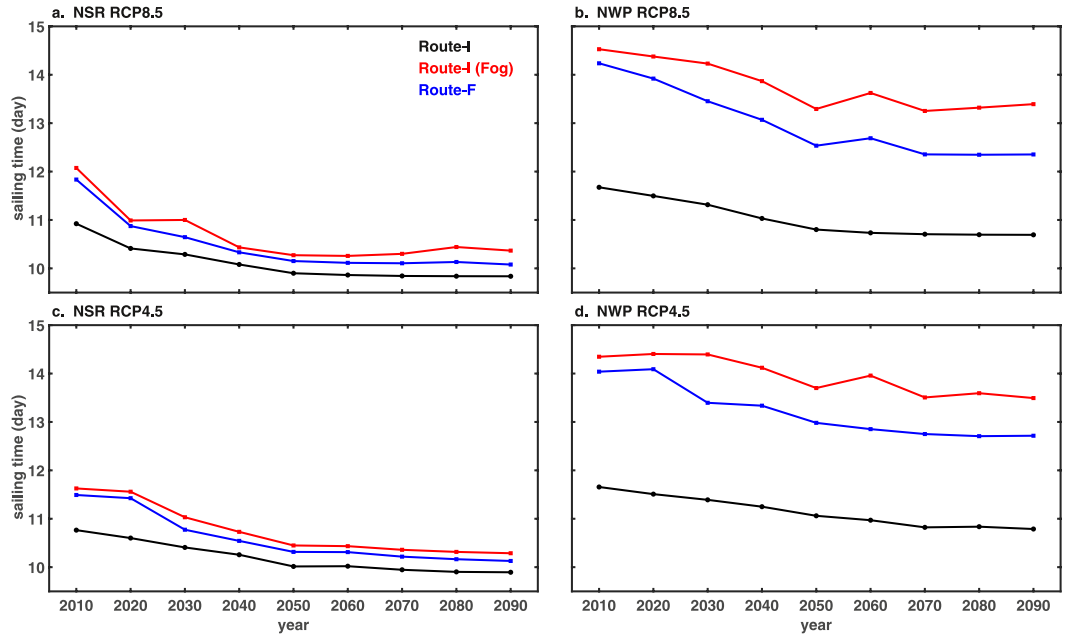

Figure 4. Sailing time along Northern Sea Route and Northwest Passage under RCP4.5 and 8.5. Black lines indicate Route-I only based on sea ice conditions; Red lines indicate Route-I but considering the deceleration of sea fog. Blue lines indicate the Route-F considering both sea ice and sea fog. The sailing time in 2010 represents the mean result during 2006–2015, and so on.

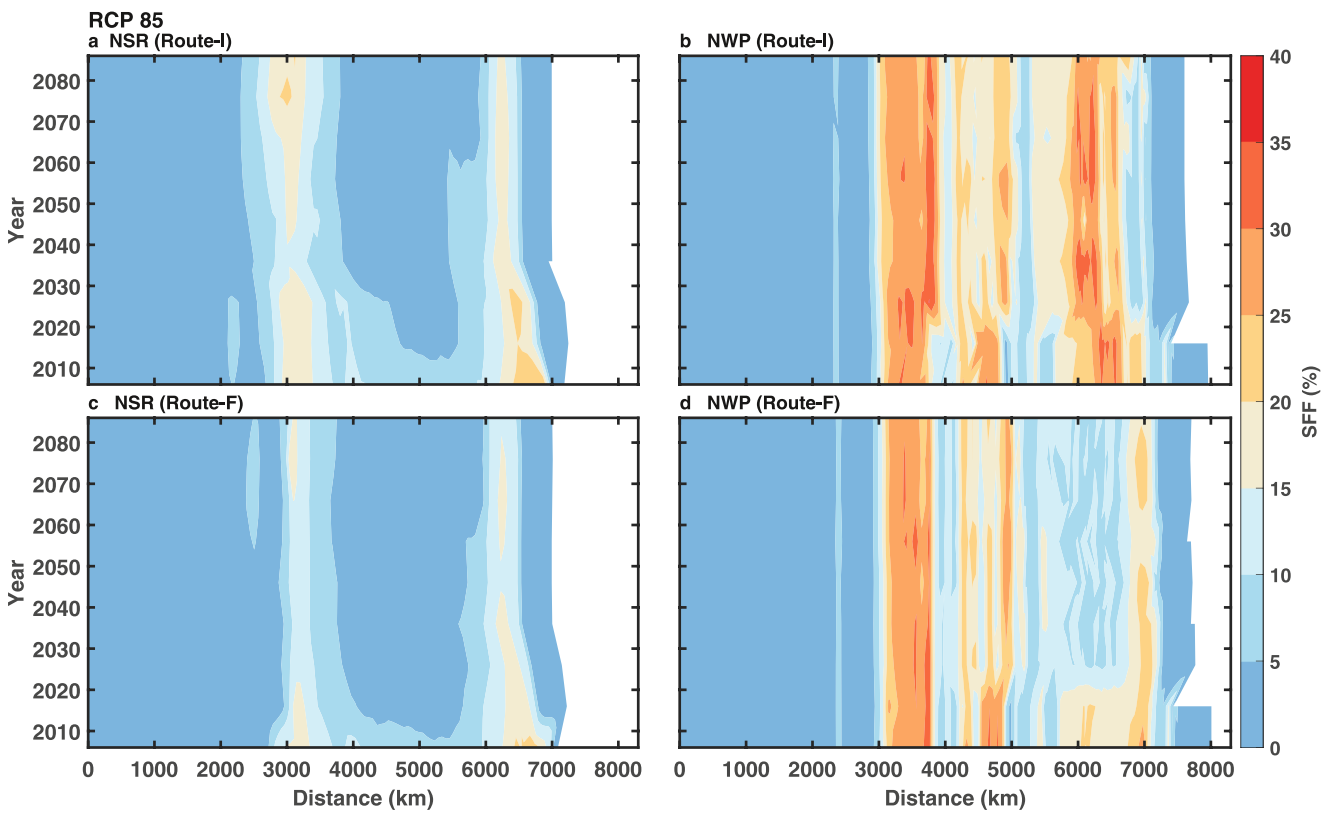

Figure 5. The variation of sea fog frequency over routes along Northern Sea Route (NSR) and Northwest Passage (NWP) under RCP8.5. The origin of NSR (NWP) is Rotterdam (St. John's). The terminals of both routes are Bering Strait.

increasing under global warming. Our result highlights the importance of Arctic sea fog when designing the trans-Arctic shipping routes in the future when Arctic sea ice continues its decline but still covers the NSR and the NWP to some extent.

The re-designed trans-Arctic shipping routes based on both sea fog and sea ice conditions over a decade window are helpful for strategic decision-making for ship operations and capacity building. Although our analysis is based on monthly data sets, and the results may not be applied directly on the operational decision-making, applying the method suggested in this analysis to real-time data can provide short-term navigation services for ship owners.

Data Availability Statement

International Comprehensive Ocean-Atmosphere Data Set (ICOADS) Observations are available from https://icoads.noaa.gov/products.html. ERA-Interim data are available from https://apps.ecmwf.int/datasets/. The Ocean Reanalysis System 5 (ORAS5) data is available at https://www.ecmwf.int/en/forecasts/dataset/ocean-reanalysis-system-5. CMIP5 data used in the paper are available from https://aims2.llnl.gov/search. The Polar WRF package is available from http://polarmet.osu.edu/PWRF/. The data and codes used in this study are available at https://doi.org/10.5281/zenodo.7789510.

Acknowledgments
X.C. was supported by the National Key R&D Program of China under Grant 2019YFA0607000, 2019YFC1509100, and Belmont Forum and the Natural Science Foundation of China under Grant 41825012 and 41561144001. J. Z. was supported by the Natural Science Foundation of China under Grant 41941012 and 41976022. KFL and KKT were supported by the Belmont Forum and the U.S. National Science Foundation through Grant NSF1536175.

References

Bintanja, R., & Selten, F. M. (2014). Future increases in Arctic precipitation linked to local evaporation and sea-ice retreat. *Nature*, *509*(7501), 479–482. https://doi.org/10.1038/nature13259

Bromwich, D. H., Hines, K. M., & Bai, L. (2009). Development and testing of polar weather research and forecasting model: 2. Arctic Ocean. *Journal of Geophysical Research*, *114*(D8), D08122. https://doi.org/10.1029/2008JD010300

Buixadé Farré, A., Stephenson, S. R., Chen, L., Czub, M., Dai, Y., Demchev, D., et al. (2014). Commercial Arctic shipping through the Northeast Passage: Routes, resources, governance, technology, and infrastructure. *Polar Geography*, *37*(4), 298–324. https://doi.org/10.1080/1088937X.2014.965769

Dee, D. P., Uppala, S. M., Simmons, A. J., Berrisford, P., Poli, P., Kobayashi, S., et al. (2011). The ERA-interim reanalysis: Configuration and performance of the data assimilation system. *Quarterly Journal of the Royal Meteorological Society*, *137*(656), 553–597. https://doi.org/10.1002/qj.828

Ducruet, C. (2013). Network diversity and maritime flows. *Journal of Transport Geography*, *30*, 77–88. https://doi.org/10.1016/j.jtrangeo.2013.03.004

Eastman, R., & Warren, S. G. (2010). Interannual variations of Arctic cloud types in relation to sea ice. *Journal of Climate*, *23*(15), 4216–4232. https://doi.org/10.1175/2010JCLI3492.1

Freeman, E., Woodruff, S. D., Worley, S. J., Lubker, S. J., Kent, E. C., Angel, W. E., et al. (2017). ICOADS release 3.0: A major update to the historical marine climate record. *International Journal of Climatology*, *37*(5), 2211–2232. https://doi.org/10.1002/joc.4775

GEF-UNDP-IMO GloMEEP Project and members of the GIA. (2020). Just in time arrival guide—Barriers and potential solutions.

Gössling, S., & Hall, M. C. (2006). *Tourism and global environmental change. Taylor & Francis*. Routledge. https://doi.org/10.4324/9780203011911

Hanesiak, J. M., & Wang, X. L. (2005). Adverse-weather trends in the Canadian Arctic. *Journal of Climate*, *18*(16), 3140–3156. https://doi.org/10.1175/JCLI3505.1

Hong, N. (2012). The melting Arctic and its impact on China's maritime transport. *Research in Transportation Economics*, *35*(1), 50–57. https://doi.org/10.1016/j.retrec.2011.11.003

Isaac, G. A., Bullock, T., Beale, J., & Beale, S. (2020). Characterizing and predicting marine fog offshore newfoundland and labrador. *Weather and Forecasting*, *35*(2), 347–365. https://doi.org/10.1175/WAF-D-19-0085.1

Koračin, D., & Dorman, C. E. (2017). In D. Koračin, & C. E. Dorman (Eds.), *Marine fog: Challenges and advancements in observations, modeling, and forecasting*. Springer International Publishing. https://doi.org/10.1007/978-3-319-45229-6

Landrum, L., & Holland, M. M. (2020). Extremes become routine in an emerging new Arctic. *Nature Climate Change*, *10*(12), 1108–1115. https://doi.org/10.1038/s41558-020-0892-z

Li, Z., Ringsberg, J. W., & Rita, F. (2020). A voyage planning tool for ships sailing between Europe and Asia via the Arctic. *Ships and Offshore Structures*, *15*(sup1), S10–S19. https://doi.org/10.1080/17445302.2020.1739369

Marko, J. R., Birch, J. R., & Wilson, M. A. (1982). A study of long-term satellite-tracked iceberg drifts in Baffin Bay and Davis Strait. *Arctic*, *35*(1), 234–240. https://doi.org/10.14430/arctic2322

Melia, N., Haines, K., & Hawkins, E. (2016). Sea ice decline and 21st century trans-Arctic shipping routes. *Geophysical Research Letters*, *43*(18), 9720–9728. https://doi.org/10.1002/2016GL069315

Munim, Z. H., Saha, R., Schøyen, H., Ng, A. K. Y., & Notteboom, T. E. (2022). Autonomous ships for container shipping in the Arctic routes. *Journal of Marine Science and Technology*, *27*(1), 320–334. https://doi.org/10.1007/s00773-021-00836-8

Nordquist, M. H., Heidar, T. H., & Moore, J. N. (2010). In *Changes in the Arctic environment and the law of the sea*. Brill.

Schøyen, H., & Bråthen, S. (2011). The northern sea route versus the Suez Canal: Cases from bulk shipping. *Journal of Transport Geography*, *19*(4), 977–983. https://doi.org/10.1016/j.jtrangeo.2011.03.003

Smith, L. C., & Stephenson, S. R. (2013). New trans-Arctic shipping routes navigable by midcentury. *Proceedings of the National Academy of Sciences of the United States of America*, *110*(13), 6–10. https://doi.org/10.1073/pnas.1214212110

Stoelinga, M. T., & Warner, T. T. (1999). Nonhydrostatic, mesobeta-scale model simulations of cloud ceiling and visibility for an East Coast winter precipitation event. *Journal of Applied Meteorology*, *38*(4), 385–404. https://doi.org/10.1175/1520-0450(1999)038<0385:NMSMSO>2.0.CO;2

Stroeve, J., Serreze, M., Drobot, S., Gearheard, S., Holland, M., Maslanik, J., et al. (2008). Arctic Sea ice extent plummets in 2007. *Eos, Transactions American Geophysical Union*, *89*(2), 13. https://doi.org/10.1029/2008EO020001

Sugimoto, S., Sato, T., & Nakamura, K. (2013). Effects of synoptic-scale control on long-term declining trends of summer fog frequency over the Pacific side of Hokkaido Island. *Journal of Applied Meteorology and Climatology*, *52*(10), 2226–2242. https://doi.org/10.1175/JAMC-D-12-0192.1

Theocharis, D., Pettit, S., Rodrigues, V. S., & Haider, J. (2018). Arctic shipping: A systematic literature review of comparative studies. *Journal of Transport Geography*, *69*, 112–128. https://doi.org/10.1016/j.jtrangeo.2018.04.010

Wagner, T. J. W., Eisenman, I., & Mason, H. C. (2021). How sea ice drift influences sea ice area and volume. *Geophysical Research Letters*, *48*(19), 1–10. https://doi.org/10.1029/2021GL093069

Wei, T., Yan, Q., Qi, W., Ding, M., & Wang, C. (2020). Projections of Arctic sea ice conditions and shipping routes in the twenty-first century using CMIP6 forcing scenarios. *Environmental Research Letters*, *15*(10), 104079. https://doi.org/10.1088/1748-9326/abb2c8

References From the Supporting Information

Clough, S. A., Shephard, M. W., Mlawer, E. J., Delamere, J. S., Iacono, M. J., Cady-Pereira, K., et al. (2005). Atmospheric radiative transfer modeling: A summary of the AER codes. *Journal of Quantitative Spectroscopy and Radiative Transfer*, *91*(2), 233–244. https://doi.org/10.1016/j.jqsrt.2004.05.058

Colbourne, D. B. (2000). Scaling pack ice and iceberg loads on moored ship shapes. *Oceanic Engineering International*, *4*(1), 39–45.

Eden, J. M., Widmann, M., Grawe, D., & Rast, S. (2012). Skill, correction, and downscaling of GCM-simulated precipitation. *Journal of Climate*, *25*(11), 3970–3984. https://doi.org/10.1175/JCLI-D-11-00254.1

Government of Canada. (2017). Arctic ice regime shipping system (AIRSS) standards. *Auvsi Xponential*, *2017*, 12259.

Grell, G. A., & Freitas, S. R. (2014). A scale and aerosol aware stochastic convective parameterization for weather and air quality modeling. *Atmospheric Chemistry and Physics*, *14*(10), 5233–5250. https://doi.org/10.5194/acp-14-5233-2014

Gultepe, I., Müller, M. D., & Boybeyi, Z. (2006). A new visibility parameterization for warm-fog applications in numerical weather prediction models. *Journal of Applied Meteorology and Climatology*, *45*(11), 1469–1480. https://doi.org/10.1175/JAM2423.1

Gultepe, I., Pearson, G., Milbrandt, J. A., Hansen, B., Platnick, S., Taylor, P., et al. (2009). The fog remote sensing and modeling field project. *Bulletin of the American Meteorological Society*, *90*(3), 341–360. https://doi.org/10.1175/2008BAMS2354.1

Guo, C., Xie, C., Zhang, J., Wang, S., & Zhao, D. (2018). Experimental investigation of the resistance performance and heave and pitch motions of ice-going container ship under pack ice conditions. *China Ocean Engineering*, *32*(2), 169–178. https://doi.org/10.1007/s13344-018-0018-9

Hines, K. M., & Bromwich, D. H. (2017). Simulation of late summer arctic clouds during ASCOS with polar WRF. *Monthly Weather Review*, *145*(2), 521–541. https://doi.org/10.1175/MWR-D-16-0079.1

Hong, S.-Y. S. S.-Y., & Lim, J.-O. (2006). The WRF single-moment 6-class microphysics scheme (WSM6). *Journal of the Korean Meteorological Society*, *42*, 129–151.

Maraun, D. (2013). Bias correction, quantile mapping, and downscaling: Revisiting the inflation issue. *Journal of Climate*, *26*(6), 2137–2143. https://doi.org/10.1175/JCLI-D-12-00821.1

Nakanishi, M., & Niino, H. (2006). An improved Mellor–Yamada level-3 model: Its numerical stability and application to a regional prediction of advection fog. *Boundary-Layer Meteorology*, *119*(2), 397–407. https://doi.org/10.1007/s10546-005-9030-8

Ngai, S. T., Tangang, F., & Juneng, L. (2017). Bias correction of global and regional simulated daily precipitation and surface mean temperature over southeast Asia using quantile mapping method. *Global and Planetary Change*, *149*, 79–90. https://doi.org/10.1016/j.gloplacha.2016.12.009

Sen, D., & Padhy, C. P. (2015). An approach for development of a ship routing algorithm for application in the North Indian Ocean region. *Applied Ocean Research*, *50*, 173–191. https://doi.org/10.1016/j.apor.2015.01.019

Teutschbein, C., & Seibert, J. (2012). Bias correction of regional climate model simulations for hydrological climate-change impact studies: Review and evaluation of different methods. *Journal of Hydrology*, *456*(457), 12–29. https://doi.org/10.1016/j.jhydrol.2012.05.052

Tong, Y., Gao, X., Han, Z., Xu, Y., Xu, Y., & Giorgi, F. (2021). Bias correction of temperature and precipitation over China for RCM simulations using the QM and QDM methods. *Climate Dynamics*, *57*(5–6), 1425–1443. https://doi.org/10.1007/s00382-020-05447-4

Woolgar, R. C., & Colbourne, D. B. (2010). Effects of hull–ice friction coefficient on predictions of pack ice forces for moored offshore vessels. *Ocean Engineering*, *37*(2–3), 296–303. https://doi.org/10.1016/j.oceaneng.2009.10.003